

# A highly magnetized environment in a pulsar binary system

<https://doi.org/10.1038/s41586-023-05983-z>

Dongzi Li<sup>1</sup>✉, Anna Bilous<sup>2</sup>, Scott Ransom<sup>3</sup>, Robert Main<sup>4</sup> & Yuan-Pei Yang<sup>5,6</sup>

Received: 7 May 2022

Accepted: 20 March 2023

Published online: 17 May 2023

 Check for updates

Spider pulsars are millisecond pulsars in short-period ( $\lesssim 12$ -h) orbits with low-mass ( $\sim 0.01\text{--}0.4 M_{\odot}$ ) companion stars. The pulsars ablate plasma from the companion star, causing time delays and eclipses of the radio emission from the pulsar. The magnetic field of the companion has been proposed to strongly influence both the evolution of the binary system<sup>1</sup> and the eclipse properties of the pulsar emission<sup>2</sup>. Changes in the rotation measure (RM) have been seen in a spider system, implying that there is an increase in the magnetic field near the eclipse<sup>3</sup>. Here we report a diverse range of evidence for a highly magnetized environment in the spider system PSR B1744 – 24A<sup>4</sup>, located in the globular cluster Terzan 5. We observe semi-regular profile changes to the circular polarization,  $V$ , when the pulsar emission passes close to the companion. This suggests that there is Faraday conversion where the radio wave tracks a reversal in the parallel magnetic field and constrains the companion magnetic field,  $B$  (>10 G). We also see irregular, fast changes in the RM at random orbital phases, implying that the magnetic strength of the stellar wind,  $B$ , is greater than 10 mG. There are similarities between the unusual polarization behaviour of PSR B1744 – 24A and some repeating fast radio bursts (FRBs)<sup>5–7</sup>. Together with the possible binary-produced long-term periodicity of two active repeating FRBs<sup>8,9</sup>, and the discovery of a nearby FRB in a globular cluster<sup>10</sup>, where pulsar binaries are common, these similarities suggest that a proportion of FRBs have binary companions.

Located in the globular cluster Terzan 5, PSR B1744 – 24A (Ter5A) is an 11.56-ms pulsar in a 1.82-h tight orbit with an approximately  $0.09 M_{\odot}$  companion<sup>4</sup>. It has been routinely observed with the 100-m Green Bank Telescope every few months for more than 15 years. The radio emission is usually eclipsed by the wind from the companion around the superior conjunction of the pulsar (at orbital phase  $\phi = 0.25$ ) when the pulsar is behind the companion. Short irregular eclipses at other orbital phases and long eclipses spanning the full orbit are also common<sup>4</sup>. These features usually last for several orbits. Here we demonstrate two uncommon polarized propagation phenomena: rapid variation in the RM at random orbital phases, and a strong change in the circular polarization near the superior conjunction.

The frequency-dependent arrival time of pulsar emission yields the foreground electron column density through dispersion measure  $DM = \int n_e dl$ , where  $n_e$  is the electron number density, and the integration  $\int dl$  is along the line of sight (LOS). Variation in polarization angle with frequency probes the foreground magnetic field, with  $RM \propto \int n_e B_{\parallel} dl$ , where  $B_{\parallel}$  is the field component parallel to the LOS. The observation at a frequency of 1.5 GHz has shown a sudden 50% decrease in RM at orbital phases of 0.65 in orbit 1 and 0.8 in orbit 2, 140° and 160° from the superior conjunction respectively, when the companion is almost behind the pulsar (Fig. 1a–d). At orbital phase 0.9 of orbit 2, about 120° away from the superior conjunction, the RM has a sudden 50% increase. A change in the sign of the  $B_{z\parallel}$  in the companion wind

should be responsible for the increase and decrease in the RM at different orbital phases. No notable variation in the DM up to  $0.01 \text{ pc cm}^{-3}$  is detected during the RM jumps, implying a lower limit of the average parallel magnetic field in the material of the companion wind;  $\langle B_z \rangle = 12 \text{ mG} (\Delta RM / 100 \text{ rad cm}^{-2}) / (\Delta DM / 0.01 \text{ pc cm}^{-3}) > 12 \text{ mG}$ . Large RM variation of greater than 3,000 rad m $^{-2}$  is expected at orbital phase  $\phi = 0.9$  in orbit 1 from this lower limit of the magnetic field, owing to the large  $\Delta DM$  of  $0.3 \text{ pc cm}^{-3}$  observed. However, the linear-polarization component ( $L$ ) drops below the noise level. Our frequency resolution should enable us to measure RM up to  $10^4 \text{ rad m}^{-2}$ , but we see RM variations of only about 100 rad m $^{-2}$ , despite much larger values being expected from the DM variation and the strong magnetic field. Linear depolarization often appears for a large fraction of the orbit, especially during regions of measurable DM variation (Fig. 1b). This depolarization is best explained by the summation of pulses with large differences in RM (see Methods). It is also possible that the unknown level of scattering has contributed to the depolarization, when different scattered paths are imparted with different RMs.

During another observation, considerable variation in the circularly polarized emission,  $V$ , was detected near the superior conjunction in three consecutive orbits recorded at 2 GHz (Figs. 1e–h and 2). Near the superior conjunction,  $V$  has the opposite sign to the unperturbed  $V$  profile, slowly turning to zero and then flipping back to the unperturbed profile as the pulsar moves away from behind the companion.

<sup>1</sup>Cahill Center for Astronomy and Astrophysics, California Institute of Technology, Pasadena, CA, USA. <sup>2</sup>ASTRON, The Netherlands Institute for Radio Astronomy, Dwingeloo, The Netherlands.

<sup>3</sup>National Radio Astronomy Observatory, Charlottesville, VA, USA. <sup>4</sup>Max-Planck-Institut für Radioastronomie, Bonn, Germany. <sup>5</sup>South-Western Institute For Astronomy Research, Yunnan University, Yunnan, China. <sup>6</sup>Purple Mountain Observatory, Chinese Academy of Sciences, Nanjing, China. ✉e-mail: dongzili@caltech.edu

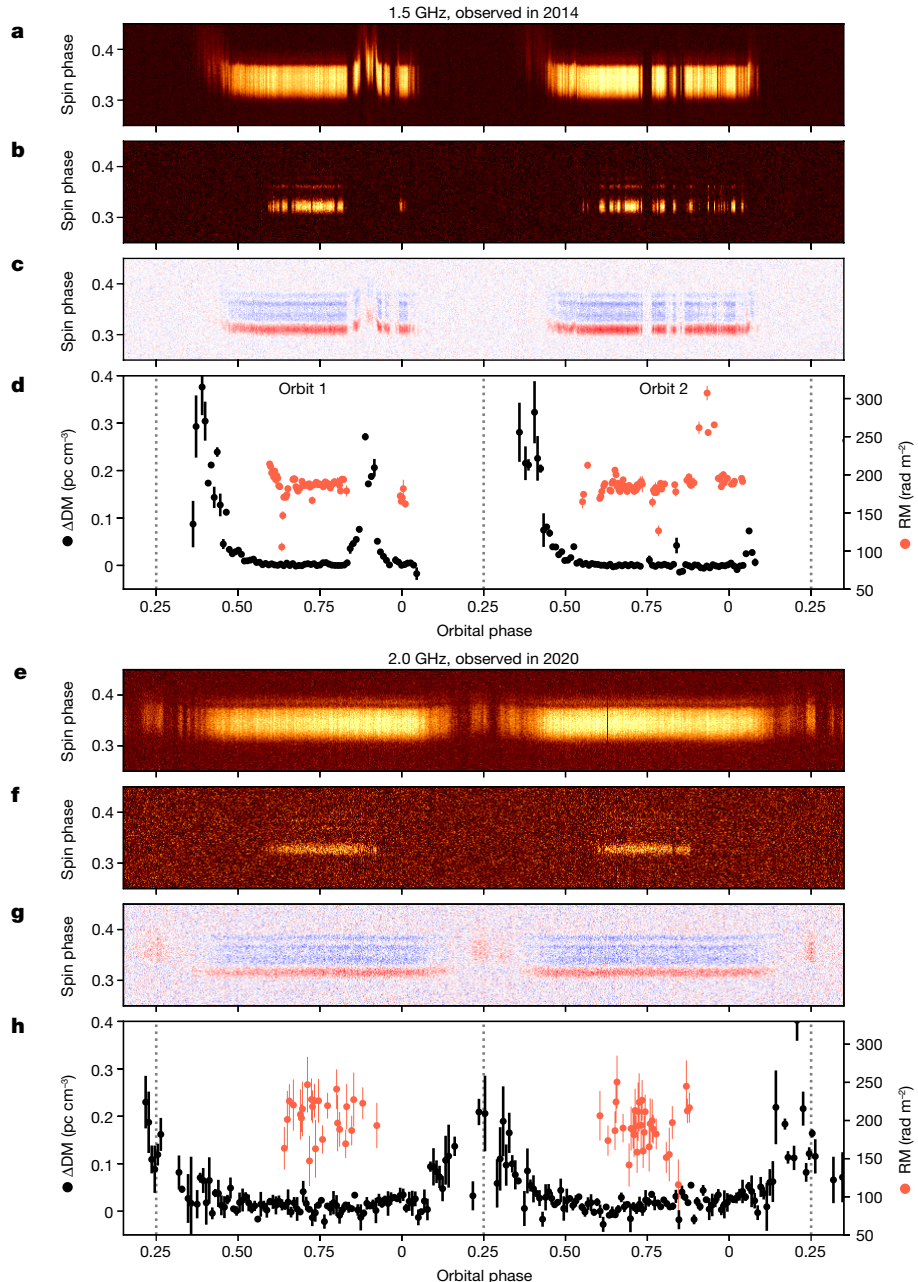


**Fig. 1 | Ter5A polarization varies considerably with orbital phase.** **a,e**, Pulse intensity ( $I$ , orange) variation against orbital phase and spin phase. **b,f**, Linear polarization ( $L$ , orange) variation against orbital and spin phase. Faraday rotation has been corrected using the fitted local value of rotation measure (RM). **c,g**, Circular polarization variation against orbital and spin phase, with red corresponding to positive values and blue to negative ones. **a–c** and **e–g** are dedispersed with a constant dispersion measure  $DM_0 = 242.36 \text{ pc cm}^{-3}$  and

folded with 512 phase bins and averaged over 20 s. **d,h**,  $\Delta DM = DM - DM_0$  in 1-min integrations (black dots) and RM in 20-s integrations (red dots). Error bars show s.d., some of which are smaller than the symbol. Dotted lines show the superior conjunction of the pulsar. Irregular, fast variations in RM, as well as depolarizations, are seen at random orbital phases owing to the magnetized plasma from the companion. Data in **a–d** were recorded at 1.5 GHz in 2014. Data in **e–h** were recorded at 2.0 GHz in 2020.

The synthetic sign reversal of  $V$  for all pulse phases, despite the different initial polarization properties, is definitive evidence of Faraday conversion where the radio wave adiabatically tracks a reversal in the parallel magnetic field  $B_z$ , an effect also known as mode coupling or tracking<sup>2,11,12</sup>.

Faraday conversion is considered to be an important mechanism to explain the recently observed circular polarization behaviour of FRB 2020124A<sup>5,13</sup>. Ter5A is an ideal system for which Faraday conversion can be unambiguously claimed. It has the advantage that the propagation effects can be isolated from the intrinsic polarization behaviour, as the latter is known from the pulse profile away from the superior conjunction. We can reproduce the complicated  $I, V$  profile

for different spin phases and frequencies, with the unperturbed profile going through a simple radio transfer function independent of the spin phase (Fig. 2d). The radio transfer function has only two components (Extended Data Fig. 2): a frequency-independent reversal of circular polarization, owing to mode-coupling Faraday conversion, and a frequency-dependent circularly polarized absorption, consistent with synchrotron–cyclotron absorption.

The Faraday conversion is best explained by the radio waves passing through the poloidal field of the companion magnetosphere with  $B > 10 \text{ G}$  ( $\Delta DM / 0.1 \text{ pc cm}^{-3})^{-1/3} (f/2 \text{ GHz})^{-4/3}$  (where  $f$  is the observation frequency) (see Methods). A reversal of the parallel magnetic field,  $B_z$ ,

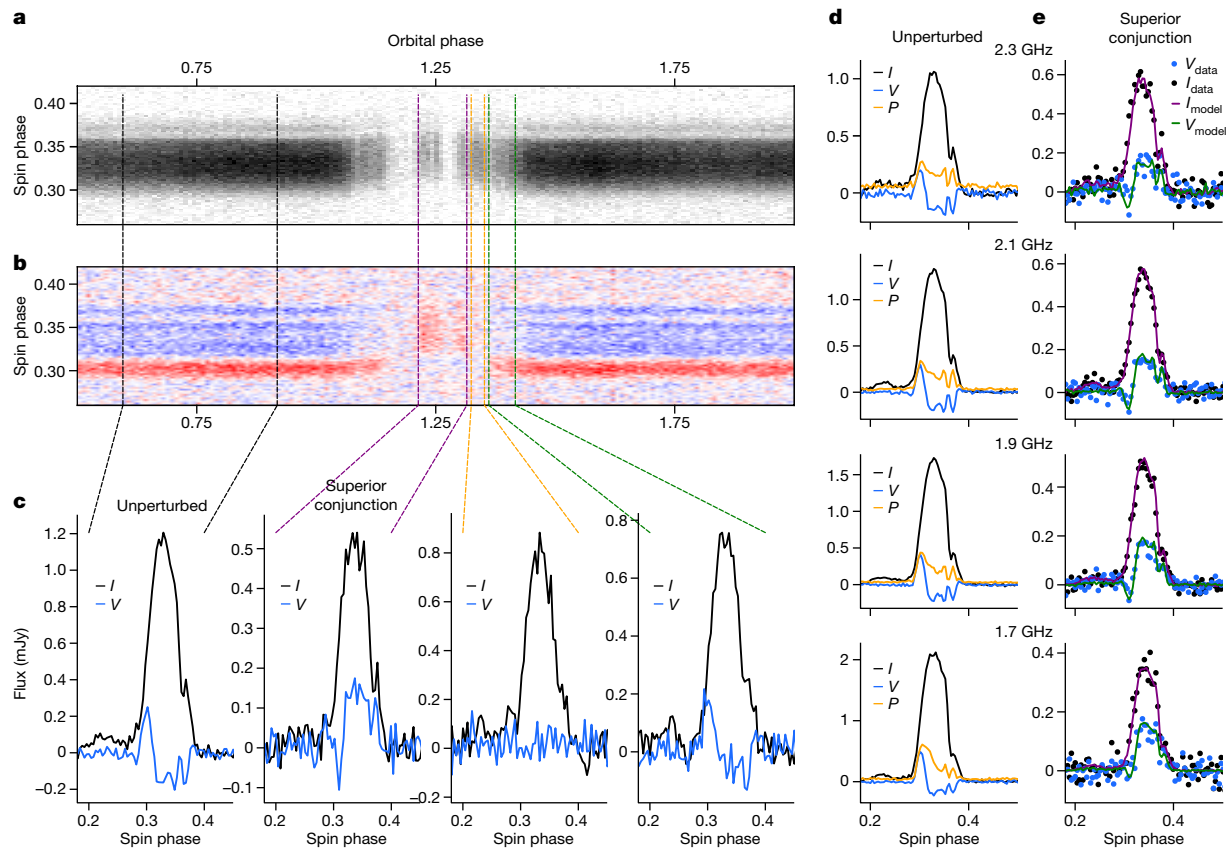


**Fig. 2 | Ter5A Faraday conversion occurs near the superior conjunction.**

**a,b**, Detailed view of the pulse intensity ( $I$ ) (**a**) and circular polarization ( $V$ ) (**b**) profiles from Fig. 1e,g,c. The emission observed in the selected orbital-phase range is averaged to produce the  $I$  (black) and  $V$  (blue) profiles against the spin phase. Between orbital phase 0.6 and 0.9 (the two black lines), the pulsar is in front of the companion and the  $I$ ,  $V$  profile does not change with the orbital phase. We averaged the pulse profile during this quiescent orbital phase and called it the unperturbed profile, which indicates pulsar polarization without the influence of the plasma from the companion.  $V$  changes sign near the superior conjunction in the orbital phase between the two purple lines. When the pulsar

moves away from the superior conjunction,  $V$  first becomes zero in the orbital phase marked by the orange lines, then changes back to the unperturbed profile in the orbital phase between the green lines. **d**, The unperturbed / ( $I$ , black),  $V$  (blue) and polarization fraction ( $P$ , orange) are shown to vary with spin phase and frequency. **e**, Observations (points) and model (lines) of the  $I$  (black) and  $V$  (blue) profiles near the superior conjunction, averaged over three orbits. The observed profiles are reproduced by the unperturbed profile in **d** going through Faraday conversion and circularly polarized absorption (see Methods).  $1 \text{ mJy} = 10^{-29} \text{ W m}^{-2} \text{ Hz}^{-1}$ .

will be experienced owing to the geometry of the large-scale poloidal field (Fig. 3), which causes  $V$  to flip near the superior conjunction in all epochs with emission not fully eclipsed. A plausible scenario for the circularly polarized absorption is synchrotron–cyclotron absorption, which suggests that  $B \approx 100 \text{ G}$  given the observed increase in the  $V$  fraction, consistent with the lower limit from the Faraday conversion (see Methods). Our model provides a qualitative prediction of  $V$  as a function of orbital phase for higher frequencies (Methods, Extended Data Fig. 3). There will be a window near  $\phi = 0.25$  over a range of frequencies where  $V$  has the opposite sign. This window becomes narrower at higher frequencies, eventually disappearing entirely. The transition region where  $V$  flips back to normal is narrow in both orbital phase and in frequency. Birefringence of lensed single pulses<sup>14,15</sup> near the superior conjunction will also be expected (see Methods). Both the Faraday conversion and the circularly polarized absorption indicate a highly magnetized companion. The orbital phase-dependent changes of the polarization profile could provide a measure of the orbital inclination angle, as the orbital geometry strongly affects the observed values of  $B$  throughout the orbit<sup>16</sup>.

Magnetized companions have been observed to introduce RM variations or a decrease in the linearly polarized flux near the periastron or superior conjunction<sup>3,17–19</sup>. Our observations of Ter5A further show that the magnetized wind of the companion can introduce order-one

RM variation even when the companion is almost behind the pulsar. When the binary system is observed edge-on, RM/DM variations close to phase 0.25 will be seen, whereas if the binary system is observed nearly face-on, irregular RM variation of both signs would be seen, depending on the intra-binary weather, which will not be strongly dependent on orbital phase.

The large, irregular RM changes are similar to those observed in FRBs, which are short, intense extragalactic radio bursts of unknown origin. Recent polarimetric studies have shown that a large fraction of FRB repeaters with more than two published RMs have shown significant RM variations<sup>5,7,20–23</sup>. Most prominently, FRB 20190520B and FRB 20201124A have shown prominent fast, irregular RM changes, which can be modelled with the existence of a companion<sup>24</sup>. Moreover, FRB 20201124A and FRB 20181112 have shown changes in circular polarization that can be attributed to either Faraday conversion or polarized absorption<sup>5,13,25</sup>. We show that these effects can also be caused by the presence of a binary companion. Moreover, the absorption mechanism responsible for the increase in the  $V$  fraction of Ter5A might also be responsible for the rare, large  $V$  observed in some FRBs<sup>5,26,27</sup>. Near the superior conjunction, the estimated  $\geq 10 \text{ G}$  field from Faraday conversion and  $\Delta \text{DM} \approx 0.2 \text{ pc cm}^{-3}$  yields an RM of  $\geq 10^6 \text{ rad m}^{-2}$ . This is even greater than the RM of FRB 20121102A<sup>20</sup>, which has one of the largest RMs of any astronomical source. The lack of detections of large RM

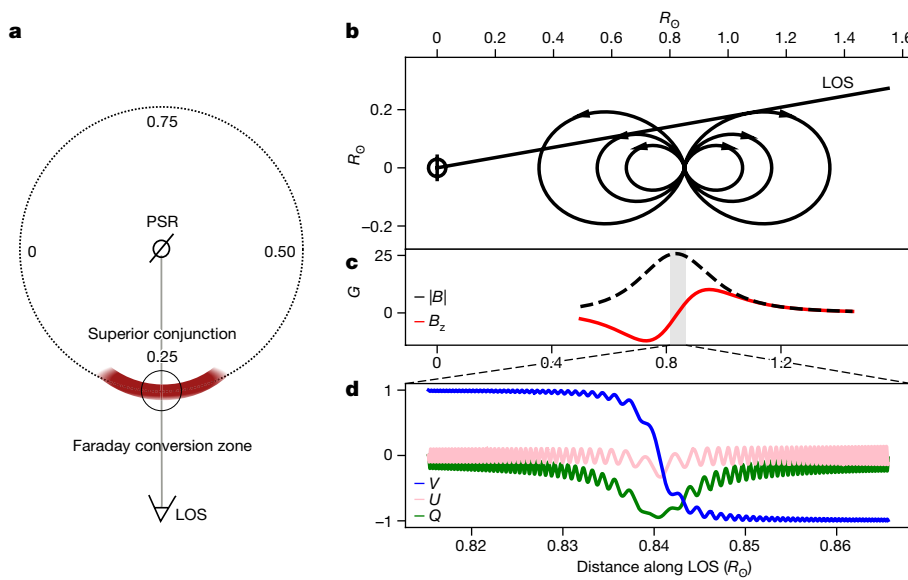


**Fig. 3 | The model of Faraday conversion in the poloidal magnetic field of the companion star.** **a**, The geometry of the orbit. Keeping the pulsar static, the companion star (small circle) orbits (dotted circle) around the pulsar (PSR). At orbital phase 0.25, the pulsar is in superior conjunction and the line of sight (LOS) is the closest to the companion. Faraday conversion is seen only at orbital phases marked with the dark red shadow. The companion and separations are drawn roughly to scale, but the pulsar is enlarged to be visible. **b**, Along the LOS at the superior conjunction, light from the pulsar passes through the poloidal field of the companion. The pulsar is located at (0,0) and the companion is at (0.85,0). The companion is assumed to be tidally locked such that the orbital and spin angular momenta are parallel. **c**, The magnetic strength  $|B|$  and parallel magnetic field  $B_z$  in the companion magnetosphere along the LOS. **d**, The change in Stokes  $Q$ ,  $U$ ,  $V$  along the LOS for the shaded region in **b**.  $V$  changes sign after passing through the region, because the radio wave adiabatically traces the field reversal. For this example, we assume that the companion has a dipole field with a dipole moment of  $2 \times 10^{32} \text{ G cm}^3$  (300 G surface field at the equator), orbital inclination angle  $i = 75^\circ$ , and an electron density  $n_e \approx \Delta DM/a \approx 5 \times 10^6 \text{ cm}^{-3}$ , where  $a$  is the orbital separation. Following equation (10), the dimensionless parameter deciding the evolution of the polarization vector  $\xi = 5$ , which is greater than 1 and hence the Faraday conversion occurs. The predicted behaviour of  $V$  against frequency and orbital phase is shown in Extended Data Fig. 3. The behaviour of  $B_z$  with a different direction of the companion magnetic axis is shown in Extended Data Fig. 1.

$B_z$  has changed its sign in the shaded region. **d**, The change in Stokes  $Q$ ,  $U$ ,  $V$  along the LOS for the shaded region in **b**.  $V$  changes sign after passing through the region, because the radio wave adiabatically traces the field reversal. For this example, we assume that the companion has a dipole field with a dipole moment of  $2 \times 10^{32} \text{ G cm}^3$  (300 G surface field at the equator), orbital inclination angle  $i = 75^\circ$ , and an electron density  $n_e \approx \Delta DM/a \approx 5 \times 10^6 \text{ cm}^{-3}$ , where  $a$  is the orbital separation. Following equation (10), the dimensionless parameter deciding the evolution of the polarization vector  $\xi = 5$ , which is greater than 1 and hence the Faraday conversion occurs. The predicted behaviour of  $V$  against frequency and orbital phase is shown in Extended Data Fig. 3. The behaviour of  $B_z$  with a different direction of the companion magnetic axis is shown in Extended Data Fig. 1.

variation in pulsar binaries with companion-induced DM changes is probably the result of depolarization arising from averaging pulses with different RMs, potentially with additional contributions from scattering (see Methods). We might be able to observe much larger RM and RM variation if single pulses, similar to those of FRBs, can be detected in the binary system.

In addition to the similarity in observed polarimetry, there is other independent evidence suggesting that some FRBs reside in binary systems. FRB 20180916B is observed to have a 16-day period<sup>8</sup>, whereas FRB 20121102A potentially has a periodicity of 160 days<sup>9,28</sup>. Binary orbits have been proposed as origins for these long-term periodicities<sup>29–32</sup>. Moreover, the spatial distribution of pulsar binaries are consistent with FRBs, which are often found to be away from star-forming regions<sup>5,33</sup>. Intriguingly, the closest extragalactic FRB, FRB 20200120E, is localized in a globular cluster<sup>10</sup>, which are dense stellar systems that are factories for compact binaries. Taken together, the evidence points to the existence of a companion star for some FRBs.

## Online content

Any methods, additional references, Nature Portfolio reporting summaries, source data, extended data, supplementary information, acknowledgements, peer review information; details of author contributions and competing interests; and statements of data and code availability are available at <https://doi.org/10.1038/s41586-023-05983-z>.

1. Ginzburg, S. & Quataert, E. Black widow evolution: magnetic braking by an ablated wind. *Mon. Not. R. Astron. Soc.* **495**, 3656–3665 (2020).
2. Thompson, C., Blandford, R. D., Evans, C. R. & Phinney, E. S. Physical processes in eclipsing pulsars: eclipse mechanisms and diagnostics. *Astrophys. J.* **422**, 304–335 (1994).
3. Crowter, K. et al. The GBT 350-MHz Drift Scan Pulsar Survey - III. Detection of a magnetic field in the eclipsing material of PSR J2256-1024. *Mon. Not. R. Astron. Soc.* **495**, 3052–3064 (2020).
4. Lyne, A. G. et al. An eclipsing millisecond pulsar in the globular cluster Terzan 5. *Nature* **347**, 650–652 (1990).
5. Xu, H. et al. A fast radio burst source at a complex magnetized site in a barred galaxy. *Nature* **609**, 685–688 (2022).
6. Luo, R. et al. Diverse polarization angle swings from a repeating fast radio burst source. *Nature* **586**, 693–696 (2020).
7. Anna-Thomas, R. et al. A highly variable magnetized environment in a fast radio burst source. Preprint at <https://arxiv.org/abs/2202.11112> (2022).
8. The CHIME/FRB Collaboration. Periodic activity from a fast radio burst source. *Nature* **582**, 351–355 (2020).
9. Rajwade, K. M. et al. Possible periodic activity in the repeating FRB 121102. *Mon. Not. R. Astron. Soc.* **495**, 3551–3558 (2020).
10. Kirsten, F. et al. A repeating fast radio burst source in a globular cluster. *Nature* **602**, 585–589 (2022).
11. Melrose, D. B., Robinson, P. A. & Feletto, T. M. Mode coupling due to twisting of magnetic field lines. *Sol. Phys.* **158**, 139–158 (1995).
12. Gruzinov, A. & Levin, Y. Conversion measure of Faraday rotation–conversion with application to fast radio bursts. *Astrophys. J.* **876**, 74 (2019).
13. Kumar, P., Shannon, R. M., Lower, M. E., Deller, A. T. & Prochaska, J. X. Propagation of a fast radio burst through a birefringent relativistic plasma. Preprint at <https://arxiv.org/abs/2204.10816> (2022).
14. Bilous, A. V., Ransom, S. M. & Demorest, P. Unusually bright single pulses from the binary pulsar B1744–24A: a case of strong lensing? *Astrophys. J.* **877**, 125 (2019).
15. Li, D. et al. Constraining magnetic fields through plasma lensing: application to the Black Widow pulsar. *Mon. Not. R. Astron. Soc.* **484**, 5723–5733 (2019).
16. Lyutikov, M. & Thompson, C. Magnetospheric eclipses in the double pulsar system PSR J0737-3039. *Astrophys. J.* **634**, 1223–1241 (2005).
17. Johnston, S. et al. Radio observations of PSR B1259-63 around periastron. *Mon. Not. R. Astron. Soc.* **279**, 1026–1036 (1996).
18. You, X. P., Manchester, R. N., Coles, W. A., Hobbs, G. B. & Shannon, R. Polarimetry of the eclipsing pulsar PSR J1748–2446A. *Astrophys. J.* **867**, 22 (2018).
19. Polzin, E. J. et al. Long-term variability of a black widow's eclipses — a decade of PSR J2051-0827. *Mon. Not. R. Astron. Soc.* **490**, 889–908 (2019).
20. Michilli, D. et al. An extreme magneto-ionic environment associated with the fast radio burst source FRB 121102. *Nature* **553**, 182–185 (2018).
21. Dai, S. et al. Magnetic field reversal around an active fast radio burst. Preprint at <https://arxiv.org/abs/2203.08151> (2022).

# Article

22. Pleunis, Z. et al. LOFAR detection of 110–188 MHz emission and frequency-dependent activity from FRB 20180916B. *Astrophys. J. Lett.* **911**, L3 (2021).
23. McKinven, R. et al. A large scale magneto-ionic fluctuation in the local environment of periodic fast radio burst source, FRB 20180916B. Preprint at <https://arxiv.org/abs/2205.09221> (2022).
24. Wang, F. Y., Zhang, G. Q., Dai, Z. G. & Cheng, K. S. Repeating fast radio burst 20201124A originates from a magnetar/Be star binary. *Nat. Commun.* **13**, 4382 (2022).
25. Cho, H. et al. Spectropolarimetric analysis of FRB 181112 at microsecond resolution: implications for fast radio burst emission mechanism. *Astrophys. J. Lett.* **891**, L38 (2020).
26. Day, C. K. et al. High time resolution and polarization properties of ASKAP-localized fast radio bursts. *Mon. Not. R. Astron. Soc.* **497**, 3335–3350 (2020).
27. Kumar, P. et al. Circularly polarized radio emission from the repeating fast radio burst source FRB 20201124A. *Mon. Not. R. Astron. Soc.* **512**, 3400–3413 (2022).
28. Cruces, M. et al. Repeating behaviour of FRB 121102: periodicity, waiting times, and energy distribution. *Mon. Not. R. Astron. Soc.* **500**, 448–463 (2021).
29. Lyutikov, M., Barkov, M. V. & Giannios, D. FRB periodicity: mild pulsars in tight O/B-star binaries. *Astrophys. J. Lett.* **893**, L39 (2020).
30. Ioka, K. & Zhang, B. A binary comb model for periodic fast radio bursts. *Astrophys. J. Lett.* **893**, L26 (2020).
31. Li, Q.-C. et al. Periodic activities of repeating fast radio bursts from Be/X-Ray binary systems. *Astrophys. J. Lett.* **918**, L5 (2021).
32. Deng, C.-M., Zhong, S.-Q. & Dai, Z.-G. An accreting stellar binary model for active periodic fast radio bursts. *Astrophys. J.* **922**, 98 (2021).
33. Tendulkar, S. P. et al. The 60 pc environment of FRB 20180916B. *Astrophys. J. Lett.* **908**, L12 (2021).

**Publisher's note** Springer Nature remains neutral with regard to jurisdictional claims in published maps and institutional affiliations.

Springer Nature or its licensor (e.g. a society or other partner) holds exclusive rights to this article under a publishing agreement with the author(s) or other rightsholder(s); author self-archiving of the accepted manuscript version of this article is solely governed by the terms of such publishing agreement and applicable law.

© The Author(s), under exclusive licence to Springer Nature Limited 2023

## Methods

### Data recording and reduction

The observations of Ter5A were recorded with the GUPPI back end on 14 October 2014 and the VEGAS back end on 21 June 2020 in an 800-MHz band centred at 1,500 MHz (L-band, session 141014) or 2,000 MHz (S-band, session 200621) in coherent dedispersion mode with a time resolution of 10.24  $\mu$ s. The signal was dedispersed in each of 512 1.56-MHz channels with the average DM of the cluster,  $DM = 238.0 \text{ pc cm}^{-3}$ . The raw data were folded according to the topocentric pulse spin period and integrated within every 20 s with dpsr. The folded profiles contained four Stokes parameters, 512 frequency channels and 512 spin phase bins (corresponding to  $t_{\text{res}} = 22.6 \mu\text{s}$ ).

Observations spanning 2010–2014 provided the initial ephemerides for folding<sup>14</sup>. For the 2020 session, ephemerides were iteratively refined using pulse times of arrivals (TOAs) away from eclipses for seven sessions in 2019–2020. TOAs were determined using single-frequency profile templates constructed from the average uneclipsed profile. Pulsar spin period, period derivative and DM were updated using all seven observations, fitting for an arbitrary phase offset between L- and S-band TOAs. Subsequently, the epoch of the ascending node, DM and projected semimajor axis were updated on a per-session basis using a Newtonian binary orbit<sup>34</sup>.

We calibrated the folded archives using standard techniques. Before each observation, a pulsed calibration signal was recorded that was used together with quasar B1442+101 as an unpolarized flux calibrator to correct for the instrumental response of the receiver system. Polarization calibration for the L-band was done using a predetermined Mueller matrix solution, which described the cross-coupling between orthogonal polarizations in the receiver<sup>35</sup>. The Mueller matrix was determined using the PSRCHIVE task pcm based on observations of PSR B0450+55. For polarization calibration in the S-band, we assumed that the feed is ideal and consists of two orthogonally polarized receptors, and the calibration signal measurements were used to balance the gain of each polarization. Such techniques were previously used for S-band observations of another millisecond pulsar, PSR B1821 – 24A<sup>36</sup>, and it proved to be adequate when comparing to more rigorous polarization calibration with predetermined Mueller matrix solutions. The complex shape of the linear polarization position angle of PSR B1821 – 24A in the S-band matched the corresponding L-band measurements within measurement uncertainty (typically a few degrees) after taking into account the influence of scattering on sharp jumps of the position angle at the lowest L-band frequencies.

The DM was measured with tempo2 by fitting the inverse-square frequency-dependent pulse arrival-time delay. To get the pulse arrival time, we correlated the pulse profile in each quarter-band subintegration with a band-integrated template if a subintegration had sufficient signal-to-noise ratio (S/N). To analyse different temporal scales of DM variation, we performed the measurement on a set of subintegrations timescales varying from 10 s to 4 min.

The RM was measured with PSRCHIVE task rmfit on 20-s subintegrations with 256 sub-bands at the L-band and, owing to the lower S/N, 128 sub-bands at the S-band. This task corrects for Faraday rotation and computes the total linear polarization on a grid of trial RMs. The optimal RM is determined by fitting a Gaussian to the peak of the obtained linear polarization fraction, with the RM uncertainty being the error of the Gaussian centroid determination. The RM is further refined with an iterative differential position angle refinement technique (<http://psrchive.sourceforge.net/manuals/rmfit/>), which compares the position angle in two halves of the observing band.

### RM variation and linear depolarization

In the quiescent phase, radio emission from Ter5A has on average 10% linear polarization with around 20% at some spin phases (see the unperturbed pulse profile in Fig. 2), which enables the measurement of RM

through Faraday rotation. In the observation at 1.5 GHz, irregular fast RM changes are observed (Fig. 1d). Various 20-s single-integration RM outliers are seen at different orbital phases, whereas at orbital phase 0.9 of orbit 2, roughly 120° away from the inferior conjunction, the RM suddenly increases by about 100 rad m<sup>-2</sup> in less than 20 s and lasts for approximately 6% of the orbit. No significant DM variation more than 0.01 pc cm<sup>-3</sup> is detected during regions displaying RM variation, giving a lower limit of the average intervening magnetic field of  $\langle B \rangle = 12 \text{ mG} (\Delta RM / 100 \text{ rad m}^{-2}) / (DM_{\text{wind}} / 0.01 \text{ pc cm}^{-3}) > 12 \text{ mG}$  at orbital phase 0.9 in orbit 2 where the pulsar is not behind the companion. Here we assume that the baseline  $DM_0 = 242.36 \text{ pc cm}^{-3}$ , commonly measured in the unperturbed phase, is contributed by the foreground, and the  $\Delta DM$  in Fig. 1 represents the excess  $DM_{\text{wind}}$  contributed by the highly variable wind. The change  $\Delta RM \propto \langle B \rangle \Delta DM + \Delta \langle B \rangle DM$ , as both  $\Delta DM$  and DM will not be larger than the measured limit of  $\Delta DM$ , so we can constrain the lower limit of the  $\langle B \rangle$ . The large changes in RM happening in less than  $\Delta t = 20 \text{ s}$  suggests either turbulent activities at an extremely short timescale, or, more likely, a small-scale structure in electron column density or magnetic field, with spatial scale  $\Delta L \lesssim v \Delta t = 0.01 R_\odot$ , where  $v \approx 800 \text{ km s}^{-1}$  is the orbital velocity assuming a neutron star mass of  $1.4 M_\odot$ .

Excess DM is observed at various orbital phases, during which the linear polarization disappears. Near orbital phase 0.9,  $\Delta DM$  rapidly increases to approximately 0.3 pc cm<sup>-3</sup>, suggesting a quick change of  $\Delta RM > 3,000 \text{ rad m}^{-2}$  given the lower limit of  $\langle B \rangle$  derived for phase 0.9 from orbit 2. However, no linear polarization is observed above the noise level. The measurement is not limited by the frequency resolution, as the frequency resolution of the data  $\Delta f = 1.56 \text{ MHz}$  should enable RM measurement all the way to  $f^3/c^2 \Delta f = 24,000 \text{ rad m}^{-2}$  and 57,000 rad m<sup>-2</sup> at 1.5 and 2 GHz, respectively. The depolarization should be a result of the fast variations of RM. Each integration is the sum of 20 s of pulses. If the pulses have passed through an RM gradient of  $\Delta RM = RM' T$  over time  $T = 20 \text{ s}$ , the linear polarization  $L$  will drop to

$$L_{\text{obs}}/L = \frac{\int_{T_0}^{T_0+T} L \exp(2iRM\lambda^2 + 2iRM't\lambda^2) dt}{\int_{T_0}^{T_0+T} L \exp(2iRM\lambda^2) dt} = \frac{\sin(\Delta RM \lambda^2)}{\Delta RM \lambda^2}. \quad (1)$$

Alternatively, if the pulses have experienced a random RM variation,  $\Delta RM$ , with s.d.  $\sigma_{\text{RM}}$ , the linear polarization  $L$  will decrease even faster<sup>37</sup>:

$$L_{\text{obs}}/L = \frac{1}{\sqrt{2} \sigma_{\text{RM}}} \int e^{2i\delta RM \lambda^2} e^{-\delta RM^2 / 2\sigma_{\text{RM}}^2} d\delta RM = e^{-2\sigma_{\text{RM}}^2 \lambda^4} \quad (2)$$

At 1.5 GHz, an RM gradient  $\Delta RM > 100 \text{ rad m}^{-2}$  or RM variation  $\sigma_{\text{RM}} > 25 \text{ rad m}^{-2}$  in the 20-s sub-integration will lead to depolarization of the observed linear polarization. This explains why no RM variations greater than -100–200 rad m<sup>-2</sup> are seen in our observations. Apart from the integration of pulses, the scattering of pulses can also introduce linear depolarization following equation (2) when different scattered paths are imparted with different RMs with s.d.  $\sigma_{\text{RM}}$ . In the case of Ter5A, no obvious scattering tail has been observed. It is possible that orders of magnitude-larger RM variations, of at least 3,000 rad m<sup>-2</sup>, can be measured with a single pulse observation.

### Faraday conversion in cold plasma

In the S-band observation, the DM increases by 0.2 pc cm<sup>-3</sup> and the circular polarization seems to have a sign reversal when the pulsar is behind the companion. The changes in the circular polarization indicate that the radio flux has gone through Faraday conversion caused by the plasma and magnetic field of the companion.

# Article

In cold plasma, assuming that the wave propagates along the  $z$  direction, the polarization vector  $\mathbf{P} = (Q, U, V)$  change follows:

$$\frac{d\mathbf{P}}{dz} = \boldsymbol{\Omega} \times \mathbf{P} \quad (3)$$

where  $\boldsymbol{\Omega} = (\rho_Q, \rho_U, \rho_V)$  and  $\rho_V$  is the Faraday rotation rate:

$$\rho_V = -\frac{2\pi}{c} \frac{f_p^2 f_B}{f^2} \hat{B}_z \quad (4)$$

where  $f_p$  is the plasma frequency and  $\rho_Q$  and  $\rho_U$  quantify the Faraday conversion rate:

$$\rho_L = \rho_Q + i\rho_U = -\frac{\pi}{c} \frac{f_p^2 f_B^2}{f^3} (\hat{B}_x + i\hat{B}_y)^2 \quad (5)$$

and where  $\hat{B} \equiv \mathbf{B}/B$ ;  $f_p = \sqrt{n_e e^2 / \pi m_e} = 9.0$  kHz ( $n_e/\text{cm}^{-3}$ )<sup>1/2</sup> is the plasma frequency,  $f_B$  is the cyclotron frequency,  $f_B = eB/2\pi m_e c = 2.8$  MHz ( $B/\text{G}$ ). This procedure can be visualized as a rotation of the polarization vector around the natural axis in the direction of  $\boldsymbol{\Omega}$  in the Poincaré sphere. We define

$$\tilde{z} \equiv 2 \frac{f}{f_B} \hat{B}_z = 2 \frac{f}{f_B} \cos \alpha \quad (6)$$

where  $\alpha$  is the pitch angle between the wave vector and the magnetic field.

When  $\tilde{z} \gg 1$ , that is,  $\rho_V \gg \rho_L$ , the natural axis  $\mathbf{n} = \boldsymbol{\Omega}/|\boldsymbol{\Omega}|$  is pointing towards the  $V$  direction, resulting in rotation of  $Q$  and  $U$ , an effect known as Faraday rotation. Faraday conversion happens when the conversion rate is similar to, or higher than, the Faraday rotation rate,  $\tilde{z} \lesssim 1$ . In this case, the natural axis  $\boldsymbol{\Omega}$  is pointing close to the linear axis, and the wave modes become quasi-linear, resulting in circular/linear conversion.

As can be seen from equations (4) and (5), the Faraday rotation rate is proportional to  $f^{-2}$ , and the Faraday conversion rate is proportional to  $f^{-3}$  for cold plasma.

For the Faraday conversion to happen, that is,  $\tilde{z} \lesssim 1$ ,  $f_B \gtrsim 2f \cos \alpha$  (equation (6)),

$$B \gtrsim 1,400 \text{ G} \left( \frac{f}{2 \text{ GHz}} \right) \cos \alpha. \quad (7)$$

Unless the pitch angle  $\alpha \approx 90^\circ$ , an extremely large magnetic field is required for Faraday conversion to happen. The phase difference between two linear eigenmodes  $\theta_f$  (the Faraday conversion angle) is:

$$\theta_f = \int \rho_L dz \approx \frac{\pi}{c} \left\langle \frac{f_p^2 f_B^2}{2f^3} \right\rangle L \quad (8)$$

$$-10^6 \text{ rad} \left\langle \left( \frac{\Delta \text{DM}}{0.1 \text{ pc cm}^{-3}} \right) \left( \frac{B}{1,000 \text{ G}} \right)^2 \left( \frac{f}{2 \text{ GHz}} \right)^{-3} \right\rangle. \quad (9)$$

Given the observed DM excess of around  $0.1 \text{ pc cm}^{-3}$ , the conversion angle is  $\gg 1$  rad. Therefore, if  $f_B \sim f$ , the circular polarization will oscillate rapidly against frequency, resulting in depolarized circular polarization with our frequency resolution. Moreover, it will require fine-tuning for a stable  $180^\circ$  conversion angle to persist across  $40^\circ$  of the orbital phase. Therefore, this scenario is inconsistent with the observation (Fig. 2).

To avoid the rapid change of conversion angle, we require  $f \gg f_B$ . In this case, Faraday conversion will occur when the magnetic field is

almost perpendicular to the LOS; in other words,  $\hat{B}_z = \cos \alpha \ll 1$  in equation (7). This would happen when there is a magnetic-field reversal.

Consider a field reversal happening at  $z = 0$ ; then we can Taylor expand  $\rho_V = \rho'_V z$ . Choosing the  $x$  axis to be the direction of the perpendicular magnetic field at the reversal, the angular frequency of the rotation can be simplified as  $\boldsymbol{\Omega} = (\rho_L, 0, \rho'_V z)$ . We define

$$\xi \equiv \frac{\rho_L^2}{\rho'_V} \approx \frac{\pi L}{2c} \frac{f_p^2 f_B^3}{f^4} \quad (10)$$

where  $L$  is the spatial scale where the magnetic field changes direction ( $|\Delta B_z| \sim |B|$ ).  $\hat{B}_x$  is omitted in the expression because  $\hat{B}_x \sim 1$  near field reversal.

Near field reversal,  $\rho'_L/\rho_L \ll \rho'_V/\rho_V$  so equation (3) can be simplified as

$$\frac{d\mathbf{P}}{\xi dz} = (1, 0, \tilde{z}) \times \mathbf{P} \quad (11)$$

If we assume that  $\rho_Q, \rho'_V$  can be considered as constants near the field reversal for  $-\tilde{z}_0 < \tilde{z} < \tilde{z}_0$ , where  $\tilde{z}_0 \gg 1$ , then the conversion angle  $\theta_f(\xi)$  depends on only  $\xi^{1/2}$

$$\theta_f(\xi) = \arccos(2 \exp(-\pi\xi/2) - 1). \quad (12)$$

With  $\xi \ll 1$ ,  $\theta_f \sim \sqrt{2\pi\xi}$ , when  $\xi \gg 1$ , the sign of the circular polarization will flip.

As shown in Fig. 2, the sign of circular polarization of the pulsar flux has reversed near the orbital phase 0.25, suggesting that  $\xi \gg 1$  near the superior conjunction where the pulsar is behind the companion. The sign reversal can persist for more than 10% of the orbital phase, corresponding to a spatial scale of  $L \sim 0.6R_\odot$  at the distance of the companion. This spatial scale is of the same order of magnitude as the size of the companion, and the Faraday conversion is repeatedly observed near the superior conjunction in all the currently processed cycles where the radio flux is not fully eclipsed. Therefore, we attribute the sign reversal to the large-scale structure of the companion. For a companion with a poloidal field, any LOS passing through the magnetosphere will experience a large-scale  $B_z$  field reversal (Fig. 3 and Extended Data Fig. 1). We can estimate the required field strength from equation (10). The DM changes by around  $0.1 \text{ pc cm}^{-3}$  during the conversion, giving a mean density of  $n_e \approx N_e/a = 5 \times 10^6 \text{ cm}^{-3}$ , where  $a = 0.85R_\odot$  is the orbital separation. It corresponds to plasma frequency  $f_p = 0.02 \text{ GHz}$ . We use the spatial scale  $L$ , where the conversion persists, as an approximation for the scale where the magnetic field changes direction. Therefore, we require an average  $B \gtrsim 10 \text{ G}$  in the magnetosphere of the companion.

## The model

Following the requirements for Faraday conversion discussed above, we construct a toy model. We assume the companion has a dipole field:

$$|B| = |M| \frac{(1 + 3\cos^2 \theta)^{1/2}}{r^3}. \quad (13)$$

Here  $|M| = B_0 r_0^3$  is the dipole moment, and  $B_0$  is the surface field at the equator,  $r_0$  is the radius of the companion, and  $\theta$  is the polar angle with  $\theta = 0^\circ$  as the equator. The change of  $|B|$  mainly depends on  $r^{-3}$ , with only a weak dependence (less than a factor of two) on polar angle  $\theta$ .

We assume the dipole moment of the companion is  $M = 2 \times 10^{32} \text{ G cm}^3$  (300 G surface field at the equator), and the LOS is offset from the axis of the orbital plane with an inclination angle  $i = 75^\circ$ . As shown in Fig. 3, the pulsar light will experience Faraday conversion near the superior conjunction. The predicted behaviour of the circular polarization  $V$  against frequency and orbital phase is shown in Extended Data Fig. 3.

In this toy model, we assume both the magnetic axis and the spin axis of the companion are parallel to the orbital axis. However, this is not essential for the appearance of the Faraday conversion. As shown in Extended Data Fig. 1, the radio wave passing across the poloidal field will inevitably experience a  $B_z$  reversal despite the direction of the magnetic axis, with the only exception being when the magnetic axis is parallel to the LOS. We specify the direction of the north magnetic pole  $P$  with longitude and latitude  $(\alpha, \delta)$ , with which the point at the equator facing the pulsar is defined to be  $(0, 0)$ . Instead of setting  $P$  at  $(90^\circ, 90^\circ)$ , as in Fig. 3a–c, we rotate the magnetic axis  $P$  to  $(180^\circ, 50^\circ)$ ,  $(0^\circ, 50^\circ)$  and  $(90^\circ, 20^\circ)$ , respectively. With the same magnetic set-up, we calculate  $\xi$  following equation (10). For all three cases,  $\xi > 1$ , which means that Faraday conversion will happen. However, the required surface field strength will differ by a factor of few to reproduce the change against orbital phase. We will leave the detailed modelling of the spin and magnetic axis of the companion for a future paper (D.Z.L. et al., manuscript in preparation).

A large magnetic field of the companion is required for Faraday conversion to happen. Although it is not known whether the  $0.089 M_\odot$  companion is an M dwarf or a white dwarf, both commonly have a large surface magnetic field<sup>38</sup>. Moreover, a magnetic field of the order of magnitude of 10 G at the contact discontinuity is expected from pressure equilibrium with the pulsar wind. The companion has been seen to eclipse the pulsar for a whole orbit, requiring a large pressure in the companion wind to withhold the pulsar wind. The pressure in the pulsar wind at the distance of the companion can be estimated from the spin down energy  $P_{\text{pw}} = \pi I \dot{P} / P^3 a^2 c$ , where  $I \sim 10^{45} \text{ g cm}^2$  is the moment of inertia of the pulsar,  $\dot{P}$  is the period derivative and  $c$  is the speed of light. The observed period derivative of Ter5A is  $\dot{P} = -1.5 \times 10^{-20} \text{ s s}^{-1}$ , which is dominated by the acceleration in the globular cluster. Given the location of the pulsar in the Terzan 5 cluster, the maximum contribution of the  $\dot{P}$  from the cluster dynamic is  $\approx 2 \times 10^{-19} \text{ s s}^{-1}$ , and both the mean and median value estimated from all the reasonable cluster models are greater than half of this value<sup>39</sup>. Taking the cluster contribution to be  $\dot{P} \sim 10^{-19} \text{ s s}^{-1}$ , the pressure of the pulsar wind at the distance of the companion is  $P_{\text{pw}} \sim 2 \text{ erg cm}^{-3}$ . To balance the pulsar wind with magnetic pressure  $P_{\text{pw}} = B_{\text{cp}}^2 / 8\pi$ , a field strength of  $B_{\text{cp}} \sim 7 \text{ G}$  in the contact discontinuity would be expected. Therefore, it is reasonable to expect the magnetic field in the companion magnetosphere to be greater than this value, and hence satisfy the condition for the Faraday conversion scenario described above.

### Modelling the Stokes $I, V$ spectrum

As shown in Fig. 2, the change of circular polarization at the top of the band (about 2.3 GHz) roughly resembles the unperturbed  $V$  profile with an opposite sign. However, in the lower half of the band ( $< 2 \text{ GHz}$ ), in addition to the flip of the sign, the  $V$  profile is shifted systematically towards a positive value. Selecting orbital phases far from the superior conjunction, where stable RM has been measured, we can measure the unperturbed linear polarization  $L$  of the pulsar, and hence can calculate the total polarization  $P = \sqrt{(L^2 + V^2)}$  (shown by the orange line in Fig. 2). Around spin phase 0.35, the circular polarization fraction near the superior conjunction exceeds the total polarization fraction in the unperturbed profile, and this trend becomes more obvious as the frequency decreases. At 1.7 GHz, the total polarization fraction  $P/I$  at spin phase 0.35 is only 15% in the unperturbed profile; however, near the superior conjunction  $V/I$  is around 50% at the same spin phase, suggesting that  $P \geq 50\%$ , which means the total polarization fraction has changed. As shown in equation (3), the total polarization fraction  $P$  is a conserved quantity in both Faraday rotation and Faraday conversion. The change of total polarization fraction against frequency, accompanied by the decrease in flux, is best explained by circularly polarized attenuation. Therefore, the radiative transfer equation (equation (3)) becomes

$$\frac{d\mathbf{S}}{ds} = -R\mathbf{S}$$

$$R = \begin{pmatrix} \eta & 0 & 0 & \eta_V \\ 0 & \eta & \rho_V & 0 \\ 0 & -\rho_V & \eta & \rho_Q \\ \eta_V & 0 & -\rho_Q & \eta \end{pmatrix} \quad (14)$$

where  $\mathbf{S} = (I, Q, U, V)$ ;  $\eta$  and  $\eta_V$  are the isotropic and circular absorption coefficients. The circular absorption happening during the adiabatic field reversal is largely cancelled. For the circular absorption happening before or after the conversion, the integrated form will be:

$$(I') = e^{-\tau} \begin{pmatrix} \cosh \tau_v & -\sinh \tau_v \\ -\sinh \tau_v & \cosh \tau_v \end{pmatrix} (I V) \quad (15)$$

where  $\tau = \eta L$ ,  $\tau_v = \eta_V L$  are the optical depth,  $C = \cos \theta_f$  is the conversion angle.

The optical depth should be frequency dependent, so we parameterize them as  $\tau = A(f/f_0)^{-\alpha}$ ,  $\tau_v = A_v(f/f_0)^{-\alpha_v}$ , where  $f_0 = 2 \text{ GHz}$ . Near the superior conjunction, the mode tracking is visually complete at the top of the band, so we fix  $C = -1$  for all of the frequencies. Using the  $I, V$  at the unperturbed phase as template  $I, V$ , we fit for the  $I', V'$  near the superior structure by varying  $A, \alpha, A_v, \alpha_v$ . The best-fit parameters are  $A = 1.08 \pm 0.01$ ,  $\alpha = -3.5 \pm 0.1$ ,  $A_v = -0.21 \pm 0.01$ ,  $\alpha_v = -3.7 \pm 0.4$ , where the error bars are the  $1\sigma$  uncertainties. The fitted curves are shown in Fig. 2e as solid lines. The separate effects of the polarized absorption and Faraday conversion on the polarization profile are shown in Extended Data Fig. 2. Although the total flux decreases after absorption,  $V$  can either increase or decrease depending on the relative sign of  $\tau_v$  and  $V$ . The complicated  $V$  profile against spin phase enables us to distinguish different propagation effects.

### Synchrotron–cyclotron absorption

Given the large magnetic field required for the Faraday conversion, synchrotron–cyclotron absorption can account for the circularly polarized absorption and varying absorption index at different orbital phases.

In the classic synchrotron limit, assuming that the relativistic electrons follow an isotropic power-law distribution  $n_r(\gamma) \propto \gamma^{-p}$  for  $\gamma_{\min} < \frac{3}{2} f_B \sin \alpha < \gamma_{\max}$ , the isotropic and circular absorption index  $\eta, \eta_V$  can be estimated with<sup>40</sup>:

$$\eta = \frac{0.08}{R_\odot^{-1} [\text{cm}^{-3}]} \frac{n_r}{\gamma_{\min}^{1-p}} \frac{(p-1)}{\Gamma\left(\frac{3p+2}{12}\right)\Gamma\left(\frac{3p+22}{12}\right)\left(\frac{3f_B \sin \alpha}{f}\right)^{p/2+1} [\text{GHz}]} \quad (16)$$

$$\eta_V = \frac{0.03}{R_\odot^{-1} [\text{cm}^{-3}]} \frac{n_r}{\gamma_{\min}^{1-p}} \frac{(p-1)}{\frac{p+3}{p+1}\Gamma\left(\frac{3p+7}{12}\right)\Gamma\left(\frac{3p+11}{12}\right)\left(\frac{3f_B \sin \alpha}{f}\right)^{p/2+3/2} [\text{GHz}]}.$$

Therefore  $\tau_v = \eta_V L \propto f^{-p/2-5/2}$  has a stronger frequency dependence compared with the isotropic optical depth  $\tau = \eta L \propto f^{-p/2-2}$ . The ratio  $\eta_v/\eta \approx 0.6 \sqrt{f_B \sin \alpha / f}$ .

We fitted  $\tau = A\left(\int/f_0\right)^{-\alpha}$ ,  $\tau_v = A_v\left(\int/f_0\right)^{-\alpha_v}$  for the pulsar flux. Near the superior conjunction, the fitted  $\alpha = -3.5 \pm 0.1$ ,  $\alpha_v = -3.7 \pm 0.4$  are consistent with  $p = 3 \pm 0.2$  from equation (16). The ratio  $\tau_v/\tau = A_v/A \approx 0.2$  at 2 GHz requires  $B \sin \alpha \sim 100 \text{ G}$ . Assuming  $\gamma_{\min} = 2$  and  $L = 0.6 R_\odot$ , the required relativistic electron density for the eclipse is  $n_r = 20 \text{ cm}^{-3}$  near the superior conjunction. The required magnetic field  $B \sim 100 \text{ G}$  is consistent with the required  $10 \text{ G} \lesssim B < 700 \text{ G}$  from the observed Faraday conversion.

# Article

The relativistic electrons also inevitably introduce linear absorption  $\eta_L$  and Faraday conversion  $\rho L^r$ . However, given  $n_e \ll n_e$  and  $f_B < f$ , these two terms will be much smaller than the Faraday rotation and conversion introduced by cold plasma (equations (4) and (5)), so their effect will not be visible.

## Observation prediction

In the scenario of Faraday conversion in the slow field reversal, for most paths, the wave is going through Faraday rotation. We can estimate the RM given the estimated magnetic field:

$$\frac{\langle \Delta \text{RM} \rangle}{[\text{rad m}^{-2}]} \sim \frac{\langle \Delta \text{DM} \rangle}{[\text{pc cm}^{-3}]} \frac{B}{[\mu\text{G}]} \quad (17)$$

Given the  $\Delta \text{DM}$  of around  $0.2 \text{ pc cm}^{-3}$ , the  $\Delta \text{RM}$  would be  $10^6 \text{ rad m}^{-2}$  for a 10-G magnetic field. The large RM would lead to a delay  $\tau_f$  between the two components of circular polarization, which may show up in the Stokes  $V$  profile:

$$\langle \tau_f \rangle = \frac{4 \langle f_B \rangle}{f} \langle \tau_p \rangle \quad (18)$$

where  $\tau_p$  is the dispersive delay, which is approximately 0.2 ms. The  $\tau_f$  would be around 10  $\mu\text{s}$  for a 10-G field. For a  $B$  strength of 10–100 G, this might lead to the suppression of Stokes parameters in the phase profile where  $V$  switches sign and there is order-one modulation on the timescale of about 100  $\mu\text{s}$ .

Observations of single pulses near the superior conjunction will be needed to verify the magnetic strength. Plasma lensing events have been seen in Ter5A<sup>14</sup>, in which single pulses can occasionally be magnified significantly. We will be able to measure the RM value of the single pulses given enough frequency resolution. Moreover, the presence of a large magnetic field will result in the left and right circular polarization of the pulse being magnified at different frequencies<sup>15</sup>. The lensing profile will be offset by a cyclotron frequency  $f_c = 2.8 \text{ MHz}$  ( $B/G$ ), which is approximately 30 MHz for  $B = 10 \text{ G}$  and about 0.3 GHz for  $B = 100 \text{ G}$ , and hence should be measurable.

Finally, we expect to see in frequency a quick transition from full conversion to no conversion, as the parameter quantifying Faraday conversion  $\xi \propto f^{-4}$ . The observation suggests that  $\xi \gg 1$  at 2 GHz (equation (10)) and hence  $|B| \gtrsim 10 \text{ G}$  near the superior conjunction. It also suggests that  $f_B \ll f$  from the frequency dependence, and hence  $|B| \ll 700 \text{ G}$ . Given that  $B \ll 700 \text{ G}$ , and that the conversion would stop happening when  $\xi \ll 1$ , the transition from full conversion to negligible conversion must happen between 2 GHz and 20 GHz (referred to as transition frequency,  $f_T$ ).  $\xi \propto f_B^3 \propto B^3$  is very sensitive to the magnetic-field strength. At different orbital phases, the LOS is passing through a different part of the magnetosphere, so we expect the transition frequency to decrease as the pulsar moves away from the superior conjunction. In summary, there will be a window near  $\Phi = 0.25$

over a range of frequencies where  $V$  has the opposite sign. This window becomes narrower at higher frequency, eventually disappearing at a certain frequency. The transition region where  $V$  flips back to normal is narrow in both orbital phase and in frequency. Using the toy model described above, we can reproduce the change of  $V$  against orbital phase for 2.3 GHz and demonstrate the expected behaviour of  $V$  at higher frequency (Extended Data Fig. 3).

## Data availability

Data are available at <https://doi.org/10.5281/zenodo.6983925>.

## Code availability

DSPSR is available at <http://dpsr.sourceforge.net> and PSRCHIVE is available at <http://psrchive.sourceforge.net>.

34. Blandford, R. & Teukolsky, S. A. Arrival-time analysis for a pulsar in a binary system. *Astrophys. J.* **205**, 580–591 (1976).
35. van Straten, W. Radio astronomical polarimetry and point-source calibration. *Astrophys. J. Suppl.* **152**, 129–135 (2004).
36. Bilous, A. V., Pennucci, T. T., Demorest, P. & Ransom, S. M. A broadband radio study of the average profile and giant pulses from PSR B1821-24A. *Astrophys. J.* **803**, 83 (2015).
37. Burn, B. J. On the depolarization of discrete radio sources by Faraday dispersion. *Mon. Not. R. Astron. Soc.* **133**, 67–83 (1966).
38. Shulyak, D. et al. Magnetic fields in M dwarfs from the CARMENES survey. *Astron. Astrophys.* **626**, A86 (2019).
39. Phinney, E. S. Pulsars as probes of newtonian dynamical systems. *Phil. Trans. R. Soc. Lond. A* **341**, 39–75 (1992).
40. Sazonov, V. N. Generation and transfer of polarized synchrotron radiation. *Soviet Astron.* **13**, 396–402 (1969).

**Acknowledgements** D.Z.L. acknowledges discussions with T. Piro, V. Ravi, H. Vedantham, U.-L. Pen, S. Phinney, J. Fuller and C. Thompson. A.B. is supported by the European Research Council under the European Union's Seventh Framework Programme (FP/2007-2013)/ERC Grant Agreement No. 617199 ('ALERT') and by the Vici research programme 'ARGO' with project number 639.043.815, financed by the Dutch Research Council (NWO). Y.-P.Y. is supported by the National Natural Science Foundation of China grant No.12003028, the National Key Research and Development Program of China (2022SKAO130101), and the China Manned Spaced Project (CMS-CSST-2021-B11). S.R. is a CIFAR fellow and is supported by the NSF Physics Frontiers Center awards 1430284 and 2020265. The National Radio Astronomy Observatory is a facility of the National Science Foundation operated under cooperative agreement by Associated Universities. The Green Bank Observatory is a facility of the National Science Foundation operated under cooperative agreement by Associated Universities.

**Author contributions** D.Z.L. modelled and interpreted the data, and prepared the majority of the manuscript. A.B. performed data pre-processing, calibration and intermediate measurements. S.R. led the data acquisition and discovered the variability of circularly polarized emission. R.M. and Y.-P.Y. helped to revise the draft and provided valuable comments.

**Competing interests** The authors declare no competing interests.

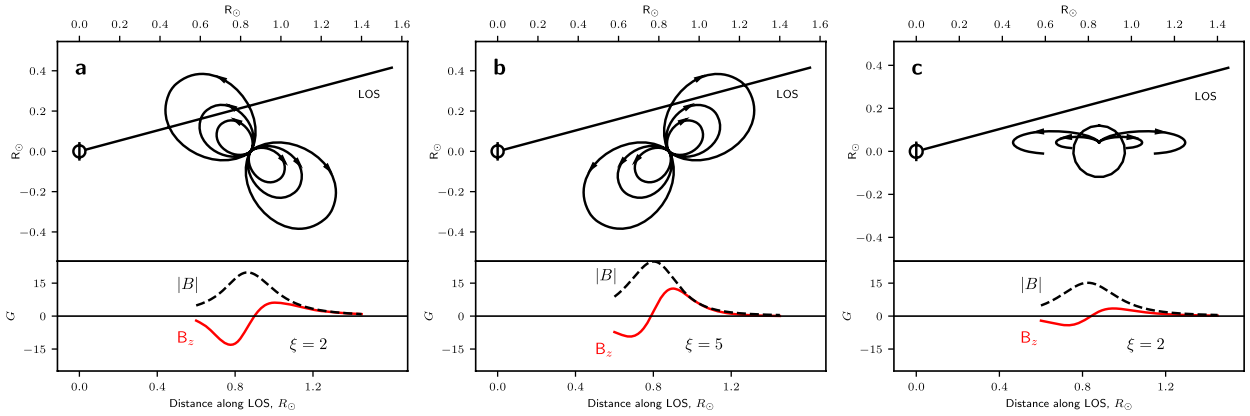
## Additional information

**Supplementary information** The online version contains supplementary material available at <https://doi.org/10.1038/s41586-023-05983-z>.

**Correspondence and requests for materials** should be addressed to Dongzi Li.

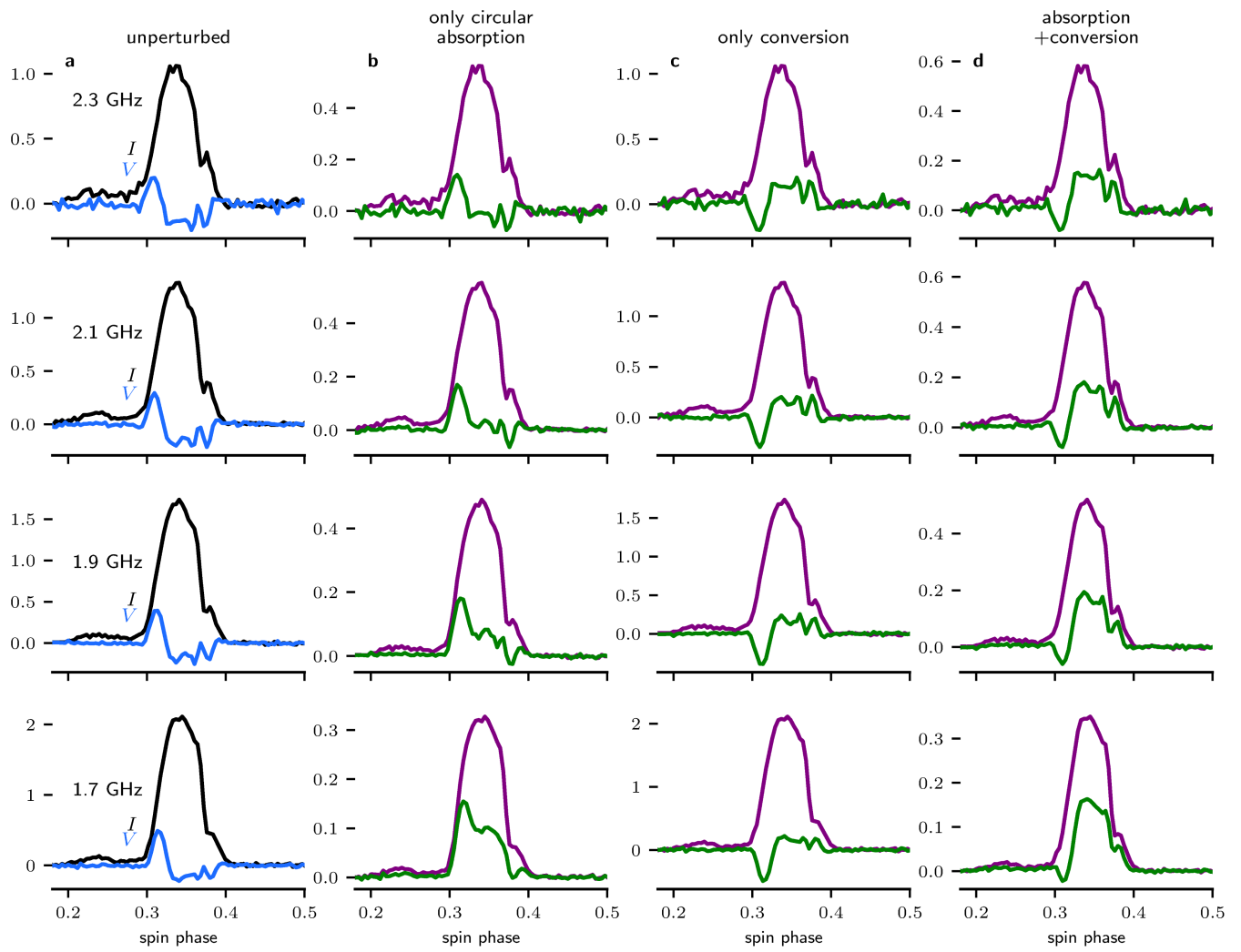
**Peer review information** *Nature* thanks the anonymous reviewers for their contribution to the peer review of this work. Peer reviewer reports are available.

**Reprints and permissions information** is available at <http://www.nature.com/reprints>.



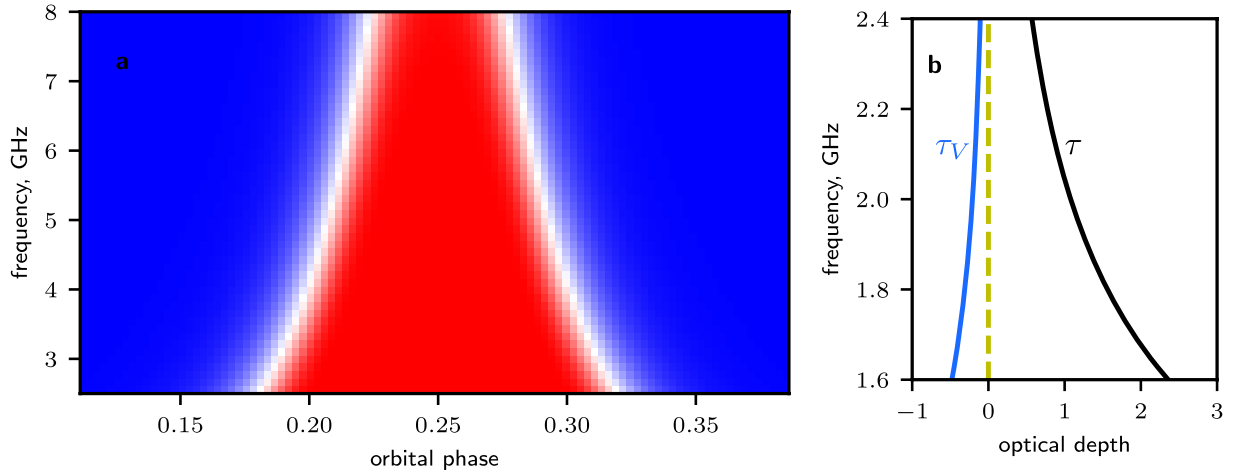
**Extended Data Fig. 1 | The large-scale  $B_{\parallel}$  reversal with various orientations of the companion magnetic axis.** We specify the direction of the north magnetic pole  $P$  with the longitude and latitude  $(\alpha, \delta)$ , with which the point at the equator facing the pulsar is defined to be  $(0, 0)$ . Panels **a**, **b** and **c** correspond to  $P$  pointing towards  $(180^\circ, 50^\circ)$ ,  $(0^\circ, 50^\circ)$  and  $(90^\circ, 20^\circ)$ , respectively. In all

cases,  $B_{\parallel}$  experiences a large-scale reversal when the  $|B|$  is around the maximum. With the same companion magnetic-field configuration as in Fig. 3, we calculate  $\xi$  following equation (10), and show that they are greater than 1 at orbit phase 0.25 in all three cases, which means that Faraday conversion will happen.



**Extended Data Fig. 2 | The individual influence of the two polarized propagation effects on the pulse profile.** We use the best-fit parameter (equation (15)) near the superior conjunction, where the degree of conversion ( $C = -1$ ,  $A = 1.1$ ,  $\alpha = -3.5$ ,  $A_v = -0.21$ ,  $\alpha_v = -3.7$ , the optical depth for  $I(\tau) = A(f/f_0)^{-\alpha}$ , the optical depth for  $V(\tau_v) = A_v \left(\frac{f}{f_0}\right)^{-\alpha_v}$ , and  $f_0 = 2$  GHz. (a) The unperturbed profile of  $I$  (black) and  $V$  (blue), which are also shown in Fig. 2d. (b,c) The model  $I$

(purple) and  $V$  (green) when the unperturbed profiles in (a) have gone through only circularly polarized absorption or Faraday conversion. (d) The joint effects of the absorption and conversion on the pulse profile. The resulting profiles are also shown in the purple and green curves in Fig. 2e, which matches the observed profiles.



**Extended Data Fig. 3 | Circular polarization varies with orbital phase and frequency.** (a) The predicted change in circular polarization,  $V$ , at higher frequency with the model in Fig. 3. The waterfall shows the  $V$  behaviour for a single spin phase, with red and blue representing different signs. Around the superior conjunction,  $\phi = 0.25$ ,  $V$  will experience Faraday conversion resulting in the change of sign. The window for Faraday conversion will become narrower at higher frequency. (b) The fitted optical depth near the superior conjunction

following equation (15). Both the total optical depth,  $\tau$ , and the circular polarization related  $\tau_V$  are decreasing fast with frequency. The modelling of circularly polarized absorption against orbital phase has more uncertainty than with Faraday conversion, owing to the unknown distribution of mildly relativistic electrons as a function of orbital phase. However, it is safe to ignore  $\tau_V$  and study the conversion against orbital phase at higher frequency, because  $\tau_V$  is already small at 2.4 GHz.